Inferring Microstructural Properties Using Angular Double Pulsed Gradient Spin Echo NMR in Orientationally Unknown Tissue

Wenjin Zhou[1], Matt G. Hall[2], and David H. Laidlaw[1]

[1] Department of Computer Science, Brown University, USA.,
[2] Department of Computer Science, University College London, UK

Abstract. We present an analytical water diffusion model for inferring important microstructural properties such as axon radius, orientation, and packing density using low-q angular Double Pulsed Gradient Spin Echo (double-PGSE) NMR, taking into account finite gradient pulses. The MR signal attenuation obtained from Single Pulsed Gradient Spin Echo (single-PGSE) NMR reflects the underlying microstructural properties that restrict the molecular diffusion within. Estimating these properties using single-PGSE, however, requires prior knowledge of axon orientation and high q-values, inhibiting clinical application of these methods. Our simulation results are the first to use low-q angular double-PGSE experiments without prior knowledge of the axon orientation to demonstrate the feasibility of estimating axon radii of the typical human brain tissue range (1 to $5\mu m$). Along with axon radius, we were also able to infer other important microstructural properties such as axon orientation, axon packing density and water diffusivity.

1 Introduction

Diffusion MRI, which measures the diffusion of spins in tissues, is a popular technique in brain research for assessing a number of neurological disorders. Current diffusion MRI brain studies rely on indirect diffusivity-based measures such as fractional anisotropy (FA) as biomarkers for major microstructural changes [1, 2]. The fact that FA is a nonspecific summation index of the observed diffusion signal over the entire voxel makes it unable to distinguish between different microstructural changes in axon radius, orientation, packing density and myelin permeability [3]. Studies have shown that neuronal changes in these microstructural properties are detected in early stages of brain diseases [4, 5] and has been observed to be location specific and axon radius size selective [6, 7]. Measuring and analyzing these specific disease-affected microstructural changes *in vivo* may provide earlier indications of brain diseases such as multiple sclerosis (MS) and Alzheimer's disease (AD).

One approach to measure axon size uses diffraction patterns of diffusion MRI signals whose frequency is related to sample compartment size [8]. This approach imposes no geometric model. Weng [9], however, showed that the measurements from diffraction patterns did not match the microscope measurements in an excised rat brain. From simulation experiments, Lätt *et al.* [10] concluded that the lowest identifiable axon radius using current scanners is $10\mu m$, while human brain axon radii usually range from 0.3 to $5\mu m$ [11].

Alternatively, microstructural properties can be extracted by constructing a geometric model of the underlying tissue in which water molecules are diffusing and analyzing the experimental MR signals [12]. Different microstructural properties can be

accounted for using the geometric model such as axon radius, packing density, orientation, etc. Assaf *et al.*[13] constructed a two-compartment CHARMED model for Single Pulsed Gradient Spin Echo (single-PGSE) experiments. In further work, they designed AxCaliber [14] to measure the Axon Diameter Distribution (ADD) of excised nerve tissues [14] and *in vivo* rat corpus callosum [15], assuming prior knowledge of axon orientation. Multi-diffusion DWI measurements let AxCaliber to classify axons using ADD since restricted diffusion is exhibited at different times relative to axon radius. Using single-PGSE approach, however, required prior knowledge of axon orientation, lengthy data acquisitions and high q-values (11 hr and $q_{max} = 51108m^{-1}$ in [14]), which can be difficult to achieve with current clinical scanners.

The Double Pulsed Gradient Spin Echo (double-PGSE) sequence (Fig. 1a) first proposed by Cory [16] has been shown to reduce eddy current distortions [17]. It contains two pairs of diffusion gradients G_1 and G_2 separated by mixing time t_m that can be applied at any angle. Mitra [18] theoretically predicted the angular dependence of signal intensity on the angle between the two gradients G_1 and G_2; this makes it possible to distinguish restricted diffusion from Gaussian diffusion, and thus to determine the sizes of axons using moderate gradient strengths with angular double-PGSE experiments. Mitra's theory, however, considered for only limiting cases of double-PGSE experiments, not taking into account finite duration of the diffusion time or mixing time. These limiting cases are difficult to achieve and Koch [19, 20] has shown that violating these conditions generally leads to underestimation of pore size and eccentricity. Özarslan [21] provided a theoretical solution for the angular dependence of NMR signal intensity in restricted geometries for arbitrary timing parameters. Shemesh [22] tested and verified this angular dependence of the signal decay [21] in well-controlled experiments using water-filled microcapillaries of known diameters ($5 - 20\mu m$).

Here, we propose an analytical water diffusion model based on Özarslan's theory [21] for inferring microstructural properties by constructing a geometric model of the underlying microstructure using low-q angular double-PGSE experiments that accounts for finite gradient pulses. Unlike single-PGSE methods [14, 15], our model does not require prior knowledge of axon orientation. We demonstrate the feasibility of estimating axon radii in typical human brain tissue ranges (1 to $5\mu m$), along with axon orientation, axon packing density, and water diffusivity with q_{max} of $25553m^{-1}$ using Monte Carlo simulation data from Camino [23, 24].

2 Methods

2.1 Analytical Model from double-PGSE

Geometric Axon Model We first construct a geometric model of the axons within which water molecules are diffusing in order to analyze the MR signal we obtain in double-PGSE experiments. Our geometric model has two compartments (Fig. 2): (1) *The intra-axonal compartment*: the space inside the axons with radius a represented by non-abutting cylinders, and (2) *The extra-axonal compartment*: the homogeneous substrate space outside the axons. These two compartments are denoted as *i* and *e* below. The boundary of the axons is assumed to be impermeable (no exchange between the two compartments).

Double-PGSE Experiments The double-PGSE sequence (Fig. 1a) is the simplest form of multi-PGSE, first proposed by Cory [16]. The double-PGSE experiments are sensitive to restricted diffusion even in the condition of long diffusion wavelength $(\gamma\delta Ga)^2 \ll 1$, also known as small-q regime $(2\pi qa)^2 \ll 1$ (where a denotes axon

radius, q denotes wave number defined as $q = \frac{\gamma \delta G}{2\pi}$, γ is the gyromagnetic ratio of the spins, δ is the pulse duration and G is the gradient strength). Özarslan [25] showed that when two diffusion gradient pulse pairs are used (as in double-PGSE), the wave number q necessary for nonmonotonicity is exactly half the wave number in single-PGSE experiments [26]. This sensitivity of the double-PGSE makes it possible to probe small compartments using relatively low wave numbers q. In a double-PGSE acquisition sequence, two encoding intervals of gradients G_1 and G_2 can be applied at any angle with an angle ψ between them. The two encoding intervals are separated by mixing time t_m with diffusion time Δ_1 and Δ_2 and pulse duration δ_1 and δ_2. Özarslan [21] theoretically predicted the angular dependence of the signal intensity on the angle between the two gradients ψ for arbitrary parameters of the double-PGSE when the long diffusion wavelength condition $(\gamma \delta G a)^2 \ll 1$ is met.

Analytical Model We propose an analytical water diffusion model aimed at estimating microstructural properties without prior knowledge of axon orientation, using angular double-PGSE based on [21]. The model analyzes the MR signal we obtain in double-PGSE experiments given the two-compartment geometric model described earlier. The intra-axonal compartment in the model exhibits restricted diffusion, while the extra-

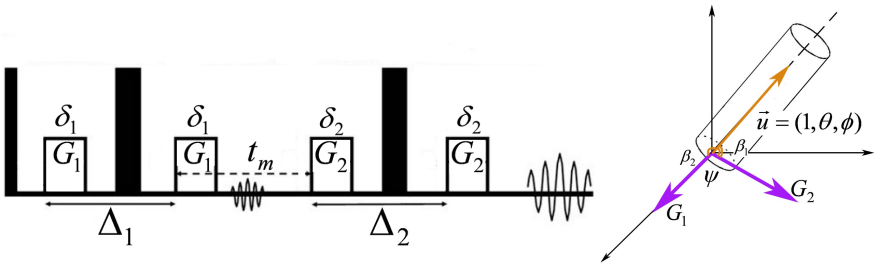

(a) Double-PGSE Acquisition Sequence (b) Experimental Setup

Fig. 1: (a) Double-PGSE acquisition sequence with two encoding intervals of gradient $\boldsymbol{G_1}$ and $\boldsymbol{G_2}$. (b) Experimental setup. $u = (1, \theta, \phi)$ defines the arbitrary axon orientation. $\boldsymbol{G_1}$ is fixed on the X-axis and $\boldsymbol{G_2}$ angle varied linearly on the XOY plane. β_1 and β_2 denote the angle between $\boldsymbol{G_1}$, $\boldsymbol{G_2}$ and $\boldsymbol{u}$ respectively.

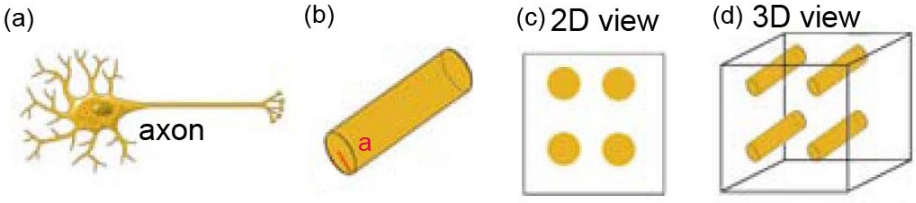

Fig. 2: Geometric axon model. (a) Schematic view of axon; (b) Single cylinder representing axon with radius a; (c-d) 2D and 3D view of non-abutting rectangular arrangement of cylinders representing axons.

axonal compartment exhibits hindered diffusion. We model the combined normalized MR signal attenuation from these two compartments as:

$$E = (1 - f)E_e + fE_i \tag{1}$$

where E_e and E_i are the normalized MR signal attenuation in the extra- and intra-axonal compartments respectively, and f is the volume fraction of the intra-axonal compartment, reflecting axon packing density.

We model the normalized MR signal attenuation in the extra-axonal compartment with Gaussian diffusion distribution:

$$E_e = e^{-\gamma^2\delta^2 D_e(G_1^2+G_2^2)(\Delta-\frac{\delta}{3})} \tag{2}$$

Here, we assume that the two encoding intervals of gradients G_1 and G_2 have the same pulse duration ($\delta_1 = \delta_2 = \delta$) and diffusion time ($\Delta_1 = \Delta_2 = \Delta$).

We further decompose the normalized MR signal attenuation in the intra-axonal compartment into two components: parallel ($E_{i//}$) and perpendicular ($E_{i\perp}$) to the axon orientation. Thus the combined MR signal attenuation in the intra-axonal compartment E_i is:

$$E_i = E_{intra//} \times E_{intra\perp} \tag{3}$$

By discretizing the gradient waveform, we can approximate it by a train of impulses using a series of propagators and derive:

$$E_{i//} = e^{-\gamma^2\delta^2 D_i(G_1^2\cos^2\beta_1+G_2^2\cos^2\beta_2)(\Delta-\frac{\delta}{3})} \tag{4}$$

$$E_{i\perp} = C + A(G_1^2\cos^2\beta_1 + G_2^2\cos^2\beta_2) - B(G_1G_2\cos\beta_1\cos\beta_2) \tag{5}$$

where,

$$C = 1 - A(G_1^2 + G_2^2) - B(G_1G_2\cos\psi) \tag{6}$$

$$A = 2\gamma^2a^2\sum_{n=1}^{\infty} S_n\left[\frac{2\delta}{\omega_n} - \frac{1}{\omega_n^2}(2 - 2e^{-\omega_n\delta} + e^{-\omega_n(\Delta-\delta)} - 2e^{-\omega_n\Delta} + e^{-\omega_n(\Delta+\delta)}\right] \tag{7}$$

$$B = 2\gamma^2a^2\sum_{n=1}^{\infty}\frac{S_n}{\omega_n^2}\Big[e^{-\omega_n(t_m-\delta)} - 2e^{-\omega_nt_m} + e^{-\omega_n(t_m+\delta)} - 2e^{-\omega_n(\Delta+t_m-\delta)} + 4e^{-\omega_n(\Delta+t_m)} - 2e^{-\omega_n(\Delta+t_m+\delta)} + e^{-\omega_n(2\Delta+t_m-\delta)} - 2e^{-\omega_n(2\Delta+t_m)} + e^{-w_n(2\Delta+t_m+\delta)}\Big] \tag{8}$$

We define:

- $s_n = \frac{1}{\alpha_n^4-\alpha_n^2}$; $w_n = \frac{\alpha_n^2 D_i}{a^2}$; α_n are the roots of the derivatives of the first-order Bessel functions satisfying the boundary condition: $J_1'(\alpha_n) = 0$
- $\cos\beta_1 = \boldsymbol{u}\cdot\boldsymbol{G_1}$ and $\cos\beta_2 = \boldsymbol{u}\cdot\boldsymbol{G_2}$, where $\boldsymbol{u} = (1, \theta, \phi)$ is the unit vector that defines the arbitrary orientation of the axon in polar coordinates (θ is the polar angle measured from the Z axis, and ϕ is the azimuth angle measured on the XOY plane from the X axis in the counter clockwise direction). β_1 and β_2 denote the angles between G_1, G_2 and $\boldsymbol{u}$ respectively. (Fig. 1b)

The experimental parameters must satisfy two conditions:

- The long diffusion wavelength condition: $(\gamma \delta G a)^2 \ll 1$.
- The diffusion time condition: $\Delta > \frac{a^2}{2D_i}$, diffusion periods must be long enough for spins to probe the boundary and experience restricted diffusion.

The axon parameters we aim to extract from the model are:

- a, the axon radius
- $u = (1, \theta, \phi)$, the axon orientation
- $f \in (0, 1)$, the volume fraction of the intra-axonal compartment
- D_i and D_e, the diffusivity of the intra- and extra-axonal compartments

2.2 Axon Parameter Estimation Procedure

Experimental Setup In order to estimate the underlying microstructural properties and validate our analytical model, we performed several simulation experiments. The benefit of using simulation data is that the ground truth about the microstructural properties is known and controllable. Figure 1a illustrates the double-PGSE sequence used in our experiment: the experimental parameters of this acquisition sequence were described in section 2.1. We assume an unknown arbitrary orientation vector $\boldsymbol{u} = (1, \theta, \phi)$ for the axon (Fig. 1b). The first gradient pair $\boldsymbol{G_1}$ is aligned on the x-axis and we varied the second gradient pair $\boldsymbol{G_2}$ in the XOY plane by changing the angle ψ between $\boldsymbol{G_1}$ and $\boldsymbol{G_2}$ and keeping their magnitude constant. In this setup, we can evaluate $\cos\beta_1 = \sin\theta\cos\phi$ and $\cos\beta_2 = \sin\theta\cos(\phi - \psi)$.

Simulation Data Our simulation data for double-PGSE experiments was derived from Monte Carlo simulation for 100,000 spins in our geometric model (section 2.1) using Camino [23, 24]. The double-PGSE sequence is simulated directly over the diffusive dynamics using a variety of scan parameters. These experiments were repeated with five different axon radii $a = (1, 2, 3, 4, 5)\mu m$ with the following axon parameters (which we later try to recover): axon orientation $\boldsymbol{u} = (30°, 60°, 1) = (\frac{\pi}{6}, \frac{\pi}{3}, 1)$; intra-axonal volume fraction $f = 0.7$; and the diffusivity of the intra- and extra-axonal compartments, assumed to be the same, $D_i = D_e = 2e^{-9}m^2/s$. Data were collected for three different q-values with experimental parameters: q_{max} of $25553m^{-1}$, pulse duration $\delta = 1.5ms$; diffusion time $\Delta = 40ms$; diffusion gradients $G_{1max} = G_{2max} = 0.4T/m$; mixing time $t_m = 5ms$; ψ varied in $10°$ increments; and SNR set to 40.

Parameter Estimation We used a Markov Chain Monte Carlo (MCMC) procedure using Gibbs sampling to get samples of the posterior distribution of the axon parameters given the simulation data and experimental parameters. The estimation procedure was implemented in MATLAB® (R2009a, The MathWorks, Natick, MA) and openBUGS [27] on Linux operating system. We used gamma distribution prior for a, beta distribution prior for f, and broad uniform priors for all the other axon parameters. Our proposed distributions were Gaussian distribution with standard deviations chosen with respect to the difference between model and experimental data. We ran MCMC for 1 million iterations with 10 sets of initial values for various parameters to ensure convergence (burn-in period = 900,000 iterations). We gathered 100,000 independent samples from the marginal posterior distribution of the model parameters as our estimates.

3 Results

Figure 3 demonstrates the accuracy of the analytical model and shows that the predicted signals from our model match the physical simulation data well in our experimental

setting. Note that (Fig. 3b) the maximum signal intensity is observed when G2 is perpendicular to the axon ($\beta_2 = 90°$), as expected [21], while holding $\boldsymbol{G_1}$ fixed on the x-axis.

Table 1 and Fig. 4 show our main results. Table 1 summarizes our estimated *mean* and standard deviation (*std*) values for axon radius a, orientation θ and ϕ, intra-axonal volume fraction f, and diffusivity D. The *mean* and *std* were calculated by averaging 100,000 samples drawn from the marginal posterior distribution of Markov Chain Monte Carlo (MCMC) (section 2.2). Figure 4 shows the histogram of axon parameter estimate packing density: a, θ, ϕ, f, D for each of the various true $a = (1, 2, 3, 4, 5)\mu m$ using MCMC. For comparison, in Fig. 4(b-e), the orange vertical lines in the graph show the true values of the corresponding axon parameters from simulation data.

We observed a slight underestimation for axons whose radius less than $3\mu m$, $a = (1, 2)\mu m$; this was also observed in [19, 20] when th SGP limits were not met using Mitra's theory [18]. It is important, however, to note that these two small axon radii recovered were still distinguishable regardless of the underestimation. We were able to recover axon radii $a = (3, 4, 5)\mu m$ with high accuracy and averaged $std = 0.0747$. As shown in table 1, the estimated values for θ, ϕ, f and D were in close agreement with their true value with $std = (0.0039, 0.0081, 0.0059, 0.0293)$ respectively. Overall, our estimation results demonstrated the feasibility of recovering axon radii in the typical human brain tissue range without prior knowledge of axon orientation.

4 Discussions

We currently run Markov Chain Monte Carlo (MCMC) sampling algorithm for 1 million iterations in order to ensure convergence for all initial values tested for each axon parameter. We could speed up MCMC chain convergence if we initialize the parameters to the true values of the simulation. We chose a longer MCMC chain to ensure conver-

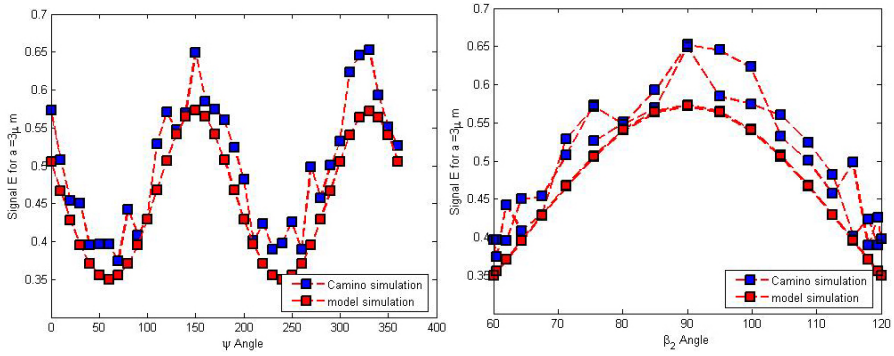

(a) Signal plotted against angle ψ (b) Signal plotted against the angle β_2

Fig. 3: Signal predicted by our model compared with Camino simulation data [28]. (a) Signal plotted against angle ψ between $\boldsymbol{G_1}$ and $\boldsymbol{G_2}$. Angle ψ ranged from $0 - 360^o$ with 10^o increments. (b) Signal plotted against the angle β_2 between $\boldsymbol{G_2}$ and axon orientation $\boldsymbol{u}$. Angle β_2 had two repeated cycles ranged from $60 - 120^o$. In this data, axon raius $a = 3\mu m$, experimental parameters were: $G = 0.4T/m$, $\delta = 1.5ms$, $\Delta = 40ms$, $t_m = 5ms$, SNR = 40.

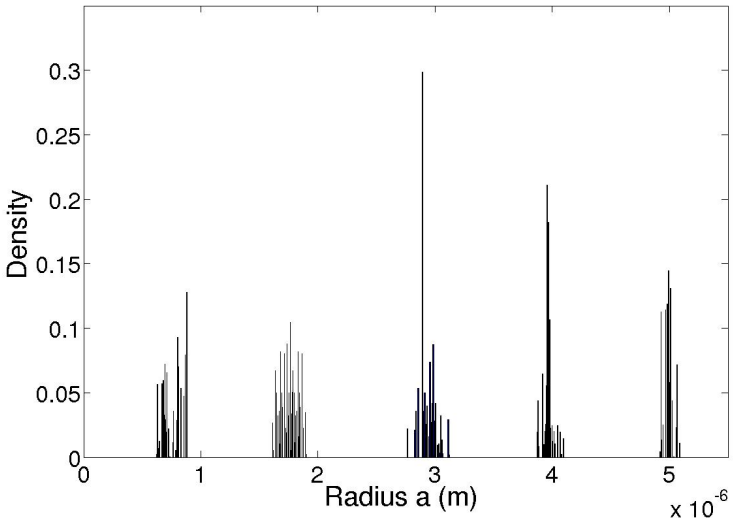

(a) Axon radius $a = (1, 2, 3, 4, 5)\mu m$

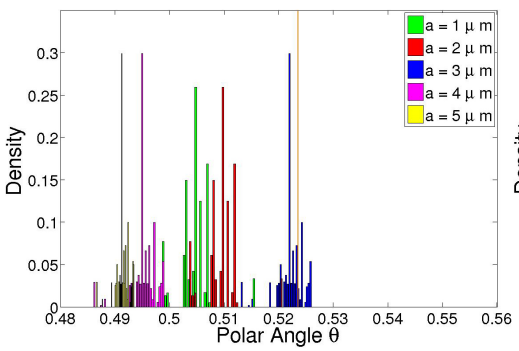

(b) Axon Polar Angle $\theta = 0.5236rad$

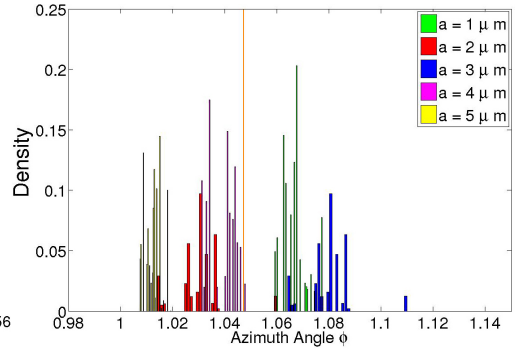

(c) Axon Azimuth Angle $\phi = 1.0472rad$

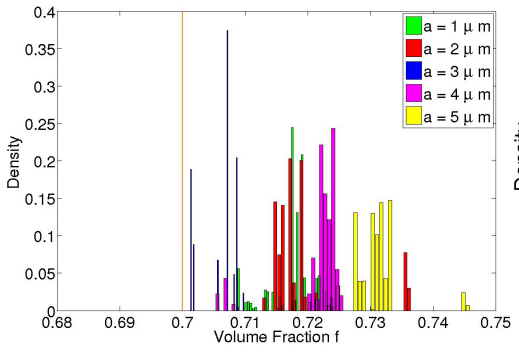

(d) Intra-axonal volume Fraction $f = 0.7$

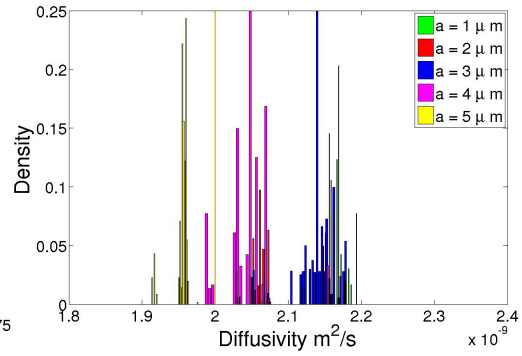

(e) Diffusivity $D = 2e^{-9}m^2/s$

Fig. 4: Histograms of 100,000 samples drawn from posterior distributions on (a) axon radius a; (b-c) axon orientation (θ and ϕ); (d) intra-axonal volume fraction $f = 0.7$; and (e) diffusivity D for each of the various true a values using Markov Chain Monte Carlo (MCMC). Orange vertical lines show the true values in simulation: $a = (1, 2, 3, 4, 5)\mu m$, $\theta = \frac{\pi}{6}rad = 30°$, $\phi = \frac{\pi}{3}rad = 60°$, $f = 0.7$, $D = 2e^{-9}m^2/s$. The *mean* and *std* values of parameter estimates are shown in table 1. Note that some overlapping bars may not be visible in the figure.

Axon radius (μm)		Axon Orientation (rad)		Volume Fraction	Diffusivity $1e^{-9}(m^2/s)$
Ground truth	Estimate	$\theta = 0.5236 = 30^\circ$	$\phi = 1.0472 = 60^\circ$	$f = 0.7$	$D = 2$
1	0.754±0.084	0.507±0.005	1.068±0.005	0.716±0.004	2.170±0.013
2	1.757±0.082	0.512±0.005	1.037±0.013	0.724±0.007	2.074±0.027
3	2.943±0.107	0.519±0.004	1.087±0.013	0.705±0.002	2.115±0.037
4	3.983±0.067	0.493±0.003	1.039±0.005	0.838±0.007	2.071±0.049
5	5.004±0.049	0.490±0.002	1.013±0.003	0.741±0.008	1.945±0.019

Table 1: Summary of estimated mean values of axon parameters from the model. Ground truth from simulation are: (a) Axon radii $a = (1, 2, 3, 4, 5)\mu m$; (b) Axon orientation; $\boldsymbol{u} = (30^\circ, 60^\circ, 1) = (\frac{\pi}{6}, \frac{\pi}{3}, 1)$; (c) Intra-axonal volume fraction $f = 0.7$; (d) Diffusivity $D = 2e^{-9}m^2/s$.

gence when we draw the last 100,000 samples of the posterior distribution regardless of the initial value, since the true parameter values are uncertain for complex white matter structures in clinical cases.

The intra-axonal volume fraction we estimate from the model is an important parameter relative to axon packing density. However, it may not directly reflect the volume fraction of the axons since only relative fractions of the axon compartment are weighted by MRI T1 and T2 relaxation [15].

The axon orientation in our model is assumed to be arbitrarily unknown but uniform based on the parallel fibers observed in the midsection of the corpus callosum. It would be interesting to look into cases of fiber crossing and kissing using spherical harmonics decomposition. In future work, we will extend our model to account for non-uniform axon caliber distribution using gamma distribution, as it has been observed in electron microscopy images. Although simple models like the diffusion tensor could describe the general axon orientation, such a model can not be used to estimate important microstructural properties such as axon radius and intra-axonal volume fraction, as the model does not encode restricted diffusion information.

5 Conclusions

We have demonstrated, for the first time without prior knowledge of the axon orientation using low-q angular double-PGSE experiments, the feasibility of estimating axon radii of the typical human brain tissue range (1 to $5\mu m$); other important underlying microstructural properties such as axon packing density and diffusivity can be extracted from the analytical model as well. Although many angles are required to achieve high angular double-PGSE resolution, these can be collected in considerably less time than multiple high-q single-PGSE experiments using the current hardware. We conclude that modeling microstructural properties using double-PGSE acquisition may be advantageous in extracting underlying microstructural properties as it requires lower q-values and has an inherently higher signal-to-noise ratio (SNR).

References

1. Pierpaoli, C., Basser, P.: Toward a quantitative assessment of diffusion anisotropy. Magnetic Resonance in Medicine **36**(6) (1996) 893–906
2. Westin, C., Maier, S., Mamata, H., Nabavi, A., Jolesz, F., Kikinis, R.: Processing and visualization for diffusion tensor MRI. Medical Image Analysis **6**(2) (2002) 93–108

3. Assaf, Y., Cohen, Y.: Inferring Microstructural Information of White Matter from Diffusion MRI. Diffusion MRI: From Quantitative Measurement to In-vivo Neuroanatomy (2009) 127
4. Lovas, G., Szilagyi, N., Majtenyi, K., Palkovits, M., Komoly, S.: Axonal changes in chronic demyelinated cervical spinal cord plaques. Brain **123**(2) (2000) 308
5. Kure, K., Weidenheim, K., Lyman, W., Dickson, D.: Morphology and distribution of HIV-1 gp41-positive microglia in subacute AIDS encephalitis. Acta Neuropathologica **80**(4) (1990) 393–400
6. Evangelou, N., Konz, D., Esiri, M., Smith, S., Palace, J., Matthews, P.: Regional axonal loss in the corpus callosum correlates with cerebral white matter lesion volume and distribution in multiple sclerosis. Brain **123**(9) (2000) 1845
7. Ganter, P., Prince, C., Esiri, M.: Spinal cord axonal loss in multiple sclerosis: a post-mortem study. Neuropathology and Applied Neurobiology **25**(6) (1999) 459–467
8. Avram, L., Assaf, Y., Cohen, Y.: The effect of rotational angle and experimental parameters on the diffraction patterns and micro-structural information obtained from q-space diffusion NMR: implication for diffusion in white matter fibers. Journal of Magnetic Resonance **169**(1) (2004) 30–38
9. Weng, J., Chen, J., Kuo, L., Wedeen, V., Tseng, W.: Maturation-dependent microstructure length scale in the corpus callosum of fixed rat brains by magnetic resonance diffusion–diffraction. Magnetic resonance imaging **25**(1) (2007) 78–86
10. Lätt, J., Nilsson, M., Malmborg, C., Rosquist, H., Wirestam, R., Stahlberg, F., Topgaard, D., Brockstedt, S.: Accuracy of q-space related parameters in MRI: simulations and phantom measurements. IEEE Transactions on Medical Imaging **26**(11) (2007) 1437
11. Edgar, J., Griffiths, I.: White Matter Structure: A Microscopists View. Diffusion MRI: From Quantitative Measurement to In-vivo Neuroanatomy (2009) 75
12. Alexander, D.: A general framework for experiment design in diffusion MRI and its application in measuring direct tissue-microstructure features. Magnetic Resonance in Medicine **60**(2) (2008) 439–448
13. Assaf, Y., Freidlin, R., Rohde, G., Basser, P.: New modeling and experimental framework to characterize hindered and restricted water diffusion in brain white matter. Magnetic Resonance in Medicine **52**(5) (2004) 965–978
14. Assaf, Y., Blumenfeld-Katzir, T., Yovel, Y., Basser, P.: AxCaliber: a method for measuring axon diameter distribution from diffusion MRI. Magnetic Resonance in Medicine **59**(6) (2008)
15. Barazany, D., Basser, P.J., Assaf, Y.: In vivo measurement of axon diameter distribution in the corpus callosum of rat brain. Brain **132** (2009) 1210–1220
16. Cory, D.G.: Applications of spin transport as a probe of local geometry. Polym. Preprints 31 **149** (1990)
17. Reese, T., Heid, O., Weisskoff, R., Wedeen, V.: Reduction of eddy-current-induced distortion in diffusion MRI using a twice-refocused spin echo. Magnetic Resonance in Medicine **49**(1) (2003) 177–182
18. Mitra, P.: Multiple wave-vector extensions of the NMR pulsed-field-gradient spin-echo diffusion measurement. Physical Review B **51**(21) (1995) 15074–15078
19. Koch, M., Finsterbusch, J.: Compartment size estimation with double wave vector diffusion-weighted imaging. Magnetic Resonance in Medicine **60**(1) (2008) 90–101
20. Koch, M., Finsterbusch, J.: Numerical simulation of double-wave vector experiments investigating diffusion in randomly oriented ellipsoidal pores. Magnetic resonance in medicine: official journal of the Society of Magnetic Resonance in Medicine/Society of Magnetic Resonance in Medicine (2009)
21. Özarslan, E., Basser, P.: Microscopic anisotropy revealed by NMR double pulsed field gradient experiments with arbitrary timing parameters. The Journal of Chemical Physics **128** (2008) 154511
22. Shemesh, N., Özarslan, E., Basser, P., Cohen, Y.: Measuring small compartmental dimensions with low-q angular double-PGSE NMR: The effect of experimental parameters on signal decay. Journal of Magnetic Resonance **198**(1) (2009) 15–23
23. Cook, P., Bai, Y., Nedjati-Gilani, S., Seunarine, K., Hall, M., Parker, G., Alexander, D.: Camino: open-source diffusion-MRI reconstruction and processing. In: 14th Scientific Meeting of the International Society for Magnetic Resonance in Medicine. (2006) 2759
24. Hall, M., Alexander, D.: Finite pulse widths improve fibre orientation estimates in diffusion tensor MRI. In: Proc. Intl. Soc. Mag. Reson. Med. Volume 14. (2006) 1076
25. Özarslan, E., Basser, P.: MR diffusion–diffraction phenomenon in multi-pulse-field-gradient experiments. Journal of Magnetic Resonance **188**(2) (2007) 285–294

26. Callaghan, P., Coy, A., MacGowan, D., Packer, K., Zelaya, F.: Diffraction-like effects in NMR diffusion studies of fluids in porous solids (1991)
27. Lunn, D., Spiegelhalter, D., Thomas, A., Best, N.: The BUGS project: Evolution, critique and future directions. Statistics in medicine **28**(25) (2009) 3049–3067
28. Hall, M., Alexander, D.: Convergence and Parameter Choice for Monte-Carlo Simulations for Diffusion MRI. IEEE transactions on medical imaging (2009)